Temperature induced crack propagation in structured media

G. Carta[a], I.S. Jones[a], M. Brun[b,c,*], N.V. Movchan[b], A.B. Movchan[b]

[a] *School of Engineering, John Moores University, Liverpool, UK*
[b] *Department of Mathematical Sciences, University of Liverpool, UK*
[c] *Dipartimento di Ingegneria Meccanica, Chimica e dei Materiali, Universita' di Cagliari, Italy*

Abstract

This paper describes the propagation of an edge crack in a semi-infinite triangular lattice, consisting of identical point masses connected by thermoelastic links. A change of temperature, represented by a time-periodic series of high-gradient temperature pulses, is applied at the boundary of the lattice. In order to make the initial crack advance in the lattice a failure criterion is imposed, whereby the links break as soon as they attain a prescribed elongation. The elongations of the links are produced both by variation in temperature and by the elastic waves generated at the boundary due to thermal shocks. The nonlinear simulations presented in this paper show that the average speed of crack propagation can be estimated from the dispersion curves of the lattice. Temperature and inertia contributions to crack propagation are also investigated. The results of this investigation show that the crack in the lattice stops at a certain distance from the boundary, and this distance depends on the frequency and amplitude of the applied temperature and on the threshold elongation. In addition, it is found that inertia amplifies the elongations of the links, and thus the crack advances further into the lattice if inertial effects are present.

Keywords: thermal striping, thermal shock, fracture, crack propagation, elastic lattice, microstructure, nonlinear problem

1. Introduction

The main cause of failure in many engineering situations is the propagation of a defect in a structural component due to the stresses generated by surface temperature fluctuations to which it is exposed. Therefore, a great deal of effort has been devoted to the study of how a crack advances in a continuum

*Corresponding author
Email addresses: giorgio_carta@unica.it (G. Carta), I.S.Jones@ljmu.ac.uk (I.S. Jones), mbrun@unica.it (M. Brun), nvm@liverpool.ac.uk (N.V. Movchan), abm@liverpool.ac.uk (A.B. Movchan)

subjected to thermal loading. The purpose of this paper is to examine the effect of microstructure on crack propagation.

Temperature oscillations occurring at the surface of a structural component may be generated by the incomplete mixing of cold and hot fluids flowing near that component. This phenomenon is known in the literature as "thermal striping", and it generally leads to structural failure by fatigue (Jones, 2005; 2006). Thermal striping is likely to take place where heat can easily transfer from the fluid to the solid component. For instance, it usually occurs in fast breeder reactors cooled by liquid sodium, where large thermal gradients exist between the sodium flows emerging from both the core and the breeder. It also occurs in pressurised water reactors, where fluids at different temperature come into contact (Jones, 2006).

Thermal striping in a continuum with an edge crack has been studied by employing several analytical approaches, such as the frequency response method (Jones and Lewis, 1994), the impulse response method (Jones and Lewis, 1996) and asymptotic analysis (Movchan and Jones, 2006). In these approaches, the thermal fatigue damage is assessed through the calculation of the fluctuation of the Stress Intensity Factor (SIF) at the crack tip. This depends both on the crack length and on the frequency of the applied temperature fluctuations (see Movchan and Jones, 2006). The SIF is usually evaluated using the weight function method (Bueckner, 1973; Jones, 1999). Nieves et al. (2011, 2012) have shown that the SIF can be reduced if additional small perforations or microcracks are present in the vicinity of the crack tip.

In situations where boundary temperature changes very rapidly in time, dynamic effects cannot be neglected, as firstly recognised by Danilovskaya (1950). This phenomenon, known as "thermal shock", may result in failure by fracture, when the SIF exceeds a critical value. Gibiansky et al. (2005) determined the asymptotic expression of the thermal stresses produced in a solid by a rapid increase of the temperature imposed on the boundary. Further work was presented by Zhelezina et al. (2006), who obtained the temperature and the thermal stress distributions over a continuum subjected to a series of pulses at the boundary and, successively, provided an asymptotic estimation of the SIF as a function of the crack depth and time.

Some aspects of crack propagation, observed experimentally, cannot be described by continuous models, but can instead be predicted if the material is assumed to be characterised by a discrete microstructure (Marder and Gross, 1995; Fineberg and Marder, 1999). In recent years a great deal of attention has been paid to discrete media, in particular to lattices. For instance, Slepyan (2001, I-III) studied the propagation of a semi-infinite crack in infinite uniform (both square and triangular) lattices and developed an analytical model from which the speed of crack propagation in the steady-state regime can be predicted. An analogous model for heterogeneous lattices was presented by Nieves et al. (2013). Colquitt et al. (2012) compared the effects of a boundary sinusoidal thermal loading in a continuum to those in the equivalent lattice, discovering that the temperature fields in the two different media are very similar, however the SIF in a continuum is larger than the corresponding quantity in

a lattice. Colquitt et al. (2012) also studied numerically the dynamic propagation of a crack in a heterogeneous triangular lattice under mechanical loads. They found that the average speed of crack propagation can be related to the dispersion curves obtained from the analytical model of Nieves et al. (2013).

The aim of the present paper is to study the dynamic propagation of an edge crack in a semi-infinite triangular lattice subjected to thermal loading. As in Zhelezina et al. (2006), temperature pulses with high gradient are imposed on the boundary of the medium. Here the medium is represented by a lattice (and not by a continuum, as in Zhelezina et al. (2006)). Colquitt et al. (2012) applied sinusoidal temperature oscillations on the lattice boundary and investigated only the steady-state conditions of the thermoelastic problem. Here the transient regime is considered and crack propagation in the medium is examined. From this study, two important results are obtained. The first one is that it is possible to estimate the speed of crack propagation in the case of thermal loads (in addition to mechanical loads, as in Colquitt et al. (2012)). The second one is that a large enough threshold elongation may lead to crack arrest in the lattice.

The layout of the paper is the following. In Section 2, the problem is formulated in detail. In Section 3, the speeds of crack propagation for different situations are obtained through a numerical procedure and they are then compared with the theoretical values derived from the analytical model developed by Slepyan (2001, III). In Section 4, the effects of temperature and inertia on crack propagation are analysed separately. In Section 5, some concluding remarks are presented. Finally, in AppendixA the solutions of the thermal problems in a continuum and in a lattice are provided and compared.

2. Description of the problem

In this paper, mode I crack propagation in a two-dimensional semi-infinite elastic lattice under thermal loading is investigated. The thermal loading is produced by a change of temperature applied on the boundary.

The lattice consists of a triangular array of point masses m connected to each other through massless links of length l, cross-sectional area A, stiffness $\mu = E\,A/l$ (where E denotes Young's modulus), coefficient of thermal expansion α and thermal diffusivity κ. The lattice is of infinite extent in x_2-direction and semi-infinite in x_1-direction, as shown in Fig. 1a. It also contains an edge crack of initial length L_0.

2.1. Governing equations

The semi-infinite lattice can be described as an array of point masses, linked by massless elastic thermally-conducting links and located at discrete positions $\mathbf{x}(\mathbf{p}) = l\mathbf{A}\mathbf{p}$, where $\mathbf{p} = (p_1, p_2)^{\mathrm{T}} \in \mathbb{Z}^2$ is the multi-index and

$$\mathbf{A} = \begin{pmatrix} 1 & 1/2 \\ 0 & \sqrt{3}/2 \end{pmatrix}. \tag{1}$$

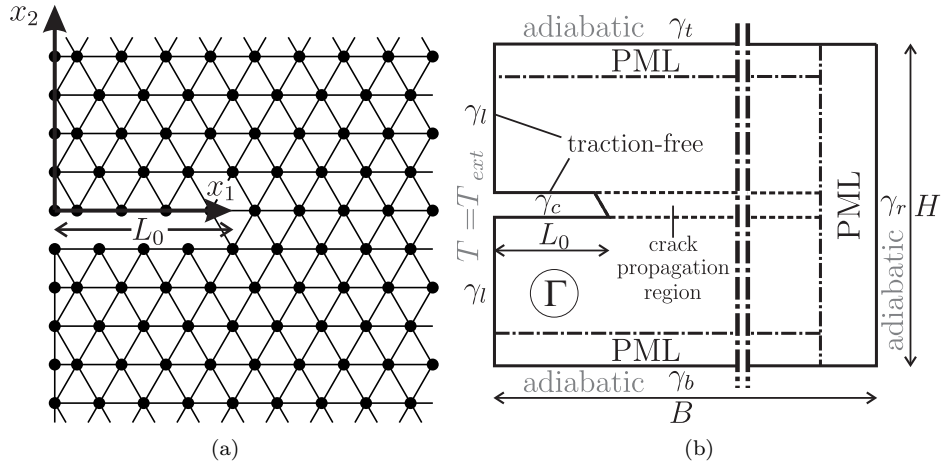

Figure 1: (a) Semi-infinite triangular lattice with a finite edge crack of length L_0. (b) Schematic drawing of the finite lattice modelled in the numerical simulations, which approximates the semi-infinite lattice in (a). Adiabatic boundary conditions and Perfectly Matched Layers (PMLs) are introduced in the model. Γ is the domain of width B and height H, while γ_l, γ_r, γ_t, γ_b and γ_c are the left, right, top, bottom and crack boundaries, respectively.

The motion of every mass in the interior of the lattice is governed by the following equations:

$$m\frac{\partial^2 \mathbf{u}(\mathbf{p},t)}{\partial t^2} = \mu \sum_{n=1}^{N(\mathbf{p})} \{\mathbf{a}_n \cdot [\mathbf{u}(\mathbf{p}+\mathbf{q}_n,t) - \mathbf{u}(\mathbf{p},t)]\,\mathbf{a}_n\} + \mathbf{F}_{\mathrm{T}}(\mathbf{p},t) \qquad \text{for } t>0; \quad (2a)$$

$$\mathbf{u}(\mathbf{p},t) = 0 \qquad \text{for } t=0; \quad (2b)$$

$$\frac{\partial \mathbf{u}(\mathbf{p},t)}{\partial t} = 0 \qquad \text{for } t=0. \quad (2c)$$

In the equations above, $\mathbf{u}(\mathbf{p},t)$ denotes the elastic displacement at time t of the particle identified by the multi-index $\mathbf{p}$, $\mathbf{q}_n$ stands for the generic node connected with a link of length l to node $\mathbf{p}$ (hence $|\mathbf{x}(\mathbf{q}_n) - \mathbf{x}(\mathbf{p})| = l$), $N(\mathbf{p})$ is the total number of nodes connected to node $\mathbf{p}$, and $\mathbf{a}_n$ is the unit vector that defines the direction of the link from $\mathbf{p}$ to $\mathbf{q}_n$. In addition, the body force $\mathbf{F}_{\mathrm{T}}(\mathbf{p},t)$ represents the thermal load, which will be derived from the uncoupled thermal problem discussed below. The boundary of the lattice and the sides of the crack are assumed to be traction-free.

For a dense enough lattice, the thermal problem can be conveniently approximated by a finite difference scheme, in which the temperature T is evaluated at the nodes and is assumed to vary linearly along the links. On the boundary, the temperature is equal to the externally imposed temperature, which will be denoted by T_{ext}. Without loss of generality, it is assumed that the ambient temperature $T_{ref} = 0$ and that it coincides with the stress-free temperature of

the material. Therefore, the thermal problem in the lattice is defined as:

$$\frac{\partial T(\mathbf{p},t)}{\partial t} = \frac{\kappa}{l^2}\left[\sum_{n=1}^{N(\mathbf{p})} T(\mathbf{q}_n,t) - N(\mathbf{p})T(\mathbf{p},t)\right] \qquad \text{for } x_1(\mathbf{p}) > 0, t > 0; \tag{3a}$$

$$T(\mathbf{p},t) = T_{ext}(t) \qquad \text{for } x_1(\mathbf{p}) = 0, t > 0; \tag{3b}$$

$$T(\mathbf{p},t) = 0 \qquad \text{for } x_1(\mathbf{p}) \geq 0, t = 0. \tag{3c}$$

The thermal load appearing in Eq. (2a) can be expressed through finite differences as

$$\mathbf{F}_{\mathrm{T}}(\mathbf{p},t) = \mu\, l\, \alpha \sum_{n=1}^{N(\mathbf{p})} \left\{[T(\mathbf{q}_n,t) - T(\mathbf{p},t)]\, \mathbf{a}_n\right\}. \tag{4}$$

2.2. Boundary temperature

The temperature imposed on the boundary of the lattice (located at $x_1 = 0$) is assumed to be uniform in the x_2 direction, and it is represented by a time-periodic series of rectangular pulses, as shown in Fig. 2. Thus, it can be expressed by the following formula:

$$T_{ext}(t) = \sum_{n=0}^{\infty} T_0\left[\mathrm{H}(t - n\,\theta) - \mathrm{H}(t - n\,\theta - \tau)\right], \tag{5}$$

where t denotes time, τ is the duration of each pulse, θ is the time interval between two consecutive pulses, $\mathrm{H}(\cdot)$ represents the Heaviside step function and T_0 is the maximum value of the applied temperature. In the rest of the paper, it will be assumed that $\theta = 4\,\tau$.

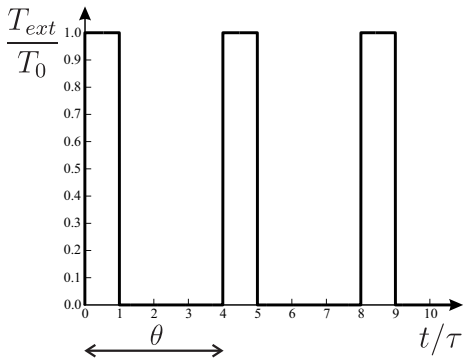

Figure 2: Time variation of the temperature imposed on the boundary $x_1 = 0$ of the lattice (with $\theta = 4\,\tau$).

Heat flows through the lattice by means of the thermally conducting links. The variation of temperature produces strains (and stresses) in the links. The latter are amplified by the elastic waves generated at the boundary due to the rapid variations of temperature, as in a continuum (Gibiansky et al., 2005; Zhelezina et al., 2006).

2.3. Numerical implementation

The thermoelastic problem is solved numerically in Comsol Multiphysics ® (version 4.2) by approximating the semi-infinite lattice with a finite lattice of width B and height H, shown schematically in Fig. 1b. In order to avoid reflections at the boundaries (which obviously cannot occur in a semi-infinite lattice), perfectly matched layers (PMLs) are implemented in the model by the introduction of viscous dampers. The latter are designed such that waves are absorbed before impinging on the boundaries. Moreover, rigid-body motion is removed from the calculations.

The temperature variation in the links is introduced into Comsol Multiphysics ® by means of the following analytic function of x_1 and t:

$$T(x_1,t)=\sum_{n=0}^{\infty}T_0\left\{\operatorname{erfc}\left[\frac{x_1}{2\sqrt{\kappa^*(t-n\,\theta)}}\right]\mathrm{H}(t-n\,\theta)\right.$$
$$\left.-\operatorname{erfc}\left[\frac{x_1}{2\sqrt{\kappa^*(t-n\,\theta-\tau)}}\right]\mathrm{H}(t-n\,\theta-\tau)\right\}, \tag{6}$$

where $\operatorname{erfc}(\cdot)$ is the complementary error function. Eq. (6) represents the solution of the heat conduction problem in a semi-infinite continuum of thermal diffusitivy κ^*, with a perfectly thermally-conducting edge crack, exposed to the boundary temperature (5). The derivation of Eq. (6) is discussed in detail in Section A.1 of AppendixA. In this appendix it is also demonstrated that the temperature distribution in the lattice, given by the finite difference scheme (3), can be efficiently approximated by the temperature distribution (6) in the continuum, provided that the thermal properties of the continuum correspond to the homogenised thermal properties of the lattice. In particular, the thermal diffusivity of the continuum κ^* has to be taken equal to the homogenised thermal diffusivity of the lattice links, i.e. $\kappa^*=\kappa\sqrt{3}$ (see Colquitt et al. (2012)). A continuum which is characterised by the homogenised properties of the lattice will be henceforth referred to as "equivalent".

The propagation of the crack is simulated in Comsol Multiphysics ® by introducing a failure criterion. More specifically, it is assumed that a link will break if it attains a threshold elongation, either in tension (stretching) or in compression (shrinking) (this symmetric type of failure is typical of many metals, in which the tensile strength is identical to the compressive strength). Buckling is not taken into account. When a link reaches the threshold elongation, the calculation is interrupted and the link is removed from the computations. The calculation is then started again by using the displacement field in the lattice at the breakage time as the initial condition for the subsequent analysis. This is how crack propagation is implemented numerically. Due to the introduction of a failure criterion, the thermoelastic problem in the lattice becomes nonlinear.

Convergence studies were carried out, which indicated that a time step of $0.02\,\tau$ is sufficiently small to get accurate results.

2.4. Normalisation

The natural units of the system, for both the elastic and thermal problems, are introduced. Firstly, two length scales are defined: the "elastic length", which is represented by the length of the lattice links l, and the "thermal length", which is given by $l_t = \sqrt{\kappa^* \tau}$. The former is a characteristic property of the lattice, while the latter is a measure of the size of the lattice region - close to the boundary - where thermal diffusion is relevant. Secondly, the speed $c = l\sqrt{\mu/m}$ is introduced. Finally, time and temperature are normalised, respectively, by the duration of each pulse τ and by the amplitude of the boundary temperature T_0. Accordingly, all the quantities used in this paper are normalised as follows:

$$\begin{aligned}
&\left(\mathbf{x}, \mathbf{u}, B, H, L_0, L, L^*, \Delta l, \Delta l_t, \frac{1}{\xi}\right) = l\left(\hat{\mathbf{x}}, \hat{\mathbf{u}}, \hat{B}, \hat{H}, \hat{L}_0, \hat{L}, \hat{L}^*, \Delta\hat{l}, \Delta\hat{l}_t, \frac{1}{\hat{\xi}}\right); \\
&\left(t, \theta, \frac{1}{\bar{\omega}}\right) = \tau\left(\hat{t}, \hat{\theta}, \frac{1}{\hat{\bar{\omega}}}\right); \qquad v = c\,\hat{v}; \qquad \omega = \frac{c}{l}\,\hat{\omega}; \\
&\left(T, T_c, T_{ref}, \frac{1}{\alpha}\right) = T_0\left(\hat{T}, \hat{T}_c, \hat{T}_{ref}, \frac{1}{\hat{\alpha}}\right).
\end{aligned} \tag{7}$$

The normalised quantities are henceforth indicated with the "hat" symbol.

By using the normalisation (7) and Eq. (4), the elastic problem stated in Eqs. (2) becomes:

$$\begin{aligned}
\frac{\partial^2\hat{\mathbf{u}}(\mathbf{p},\hat{t})}{\partial\hat{t}^2} = \quad & \frac{c^2\tau^2}{l^2}\sum_{n=1}^{N(\mathbf{p})}\left\{\mathbf{a}_n\cdot\left[\hat{\mathbf{u}}(\mathbf{p}+\mathbf{q}_n,\hat{t})-\hat{\mathbf{u}}(\mathbf{p},\hat{t})\right]\mathbf{a}_n\right\} \\
& + \frac{c^2\tau^2}{l^2}\,\hat{\alpha}\,T_0\sum_{n=1}^{N(\mathbf{p})}\left\{\left[\hat{T}(\mathbf{q}_n,\hat{t})-\hat{T}(\mathbf{p},\hat{t})\right]\mathbf{a}_n\right\} \qquad \text{for } \hat{t}>0; \quad \text{(8a)} \\
\hat{\mathbf{u}}(\mathbf{p},\hat{t}) = 0 \qquad & \text{for } \hat{t}=0; \quad \text{(8b)} \\
\frac{\partial\hat{\mathbf{u}}(\mathbf{p},\hat{t})}{\partial\hat{t}} = 0 \qquad & \text{for } \hat{t}=0. \quad \text{(8c)}
\end{aligned}$$

The thermal problem (3) is changed into the following set of equations:

$$\begin{aligned}
\frac{\partial\hat{T}(\mathbf{p},\hat{t})}{\partial\hat{t}} = \frac{\Lambda^2}{\sqrt{3}}\left[\sum_{n=1}^{N(\mathbf{p})}\hat{T}(\mathbf{q}_n,\hat{t}) - N(\mathbf{p})\hat{T}(\mathbf{p},\hat{t})\right] \qquad & \text{for } \hat{x}_1(\mathbf{p})>0, \hat{t}>0; \quad \text{(9a)} \\
\hat{T}(\mathbf{p},\hat{t}) = \hat{T}_{ext}(\hat{t}) \qquad & \text{for } \hat{x}_1(\mathbf{p})=0, \hat{t}>0; \quad \text{(9b)} \\
\hat{T}(\mathbf{p},\hat{t}) = 0 \qquad & \text{for } \hat{x}_1(\mathbf{p})\geq 0, \hat{t}=0. \quad \text{(9c)}
\end{aligned}$$

Here Λ is the ratio between the thermal length and the elastic length, i.e. $\Lambda = l_t/l$.

Finally, Eqs. (5) and (6) become

$$\hat{T}_{ext}(\hat{t}) = \sum_{n=0}^{\infty}\left[\mathrm{H}(\hat{t}-4\,n) - \mathrm{H}(\hat{t}-4\,n-1)\right] \tag{10}$$

and

$$\hat{T}(\hat{x}_1,\hat{t}) = \sum_{n=0}^{\infty} \left\{ \operatorname{erfc}\left[\frac{\hat{x}_1}{2\Lambda\sqrt{\hat{t}-4\,n}}\right] \mathrm{H}(\hat{t}-4\,n) \right. \\ \left. -\operatorname{erfc}\left[\frac{\hat{x}_1}{2\Lambda\sqrt{\hat{t}-4\,n-1}}\right] \mathrm{H}(\hat{t}-4\,n-1) \right\}, \tag{11}$$

respectively.

3. Speed of crack propagation in the lattice

In this section, it is investigated how the initial crack of length L_0, shown in Figs. 1a and 1b, propagates in the lattice due to the temperature pulses applied on the boundary. In particular, the speed of crack propagation is evaluated numerically, and it is then compared with the theoretical value derived from the dispersion diagram of the lattice given by Slepyan (2001, III).

3.1. Lattice and temperature properties

As in Slepyan (2001, III), the elastic properties of the lattice are assigned unit values, i.e. $l = 1$ and $c = 1$. The width and height of the lattice are taken as $\hat{B} = 80$ and $\hat{H} = 21\sqrt{3}/2$, respectively.

The product $\hat{\alpha}\,T_0$ is fixed, given by $\hat{\alpha}\,T_0 = -0.01$, as $\hat{\alpha}$ is typically a small quantity. Since $\hat{\alpha} > 0$, then this implies that $T_0 < 0$. A negative temperature avoids a situation of potential crack closure.

The duration of each pulse is assumed to be $\tau = 1$. Since the period of the temperature pulses is $\theta = 4\,\tau$, the fundamental radian frequency of the imposed temperature is $\hat{\hat{\omega}} = \pi/2$. The thermal length is assumed to be $l_t = 1$, which implies that $\Lambda = 1$.

Next, the initial length of the crack $\hat{L}_0$ needs to be chosen. If $\hat{L}_0$ is of the same order of magnitude as the thermal length l_t, the thermal diffusivity effects cannot be ignored. For a continuum, Zhelezina et al. (2006) showed that the stress waves generated by a series of temperature pulses applied on the boundary consist of two terms, the first one representing a plane wave (which propagates in the medium) and the second one corresponding to thermal diffusion (see Eqs. (26) and (27) in that paper). The second contribution is of importance near the boundary, in a region denoted as the "boundary layer". These two contributions can be identified also in a lattice, as will be shown in Section 4. In the present section, attention is focused on the speed of crack propagation, which will be related to the speed of the waves. Therefore, the position of the crack tip is assumed to be located far enough from the boundary to disregard the contribution of thermal diffusion. In particular, $\hat{L}_0$ is taken as $\hat{L}_0 = 20$.

3.2. Analytical model for the assessment of the crack propagation speed

The average speed of crack propagation in the homogeneous lattice of Fig. 1a can be estimated by means of a linear model developed by Slepyan (2001, III). This involves the reduction of the elastic problem of an infinite triangular lattice with a semi-infinite crack to a Wiener-Hopf equation. The dispersion relations, obtained from the poles and the zeros of the kernel of this equation, can be used to evaluate the speed of crack propagation produced by a generic harmonic load of a certain frequency. It is important to stress that Slepyan's approach assumes that the crack propagates with constant speed in a straight line, i.e. with no crack branching.

There are three dispersion relations found by Slepyan (2001, III) for mode I crack propagation:

$$\bullet \text{ Rayleigh wave:} \qquad \hat{\omega} = \sqrt{3-\sqrt{3}}\left|\sin\left(\hat{\xi}/2\right)\right|; \tag{12a}$$

$$\bullet \text{ longitudinal wave:} \qquad \hat{\omega} = \sqrt{3-\cos\left(\hat{\xi}/2\right)-2\cos\left(\hat{\xi}\right)}; \tag{12b}$$

$$\bullet \text{ optical branch:} \qquad \hat{\omega} = \sqrt{6}\left|\cos\left(\hat{\xi}/4\right)\right|. \tag{12c}$$

Here $\hat{\omega}$ and $\hat{\xi}$ represent the fundamental radian frequency and the wavenumber, respectively. The corresponding dispersion curves are reproduced in Fig. 3.

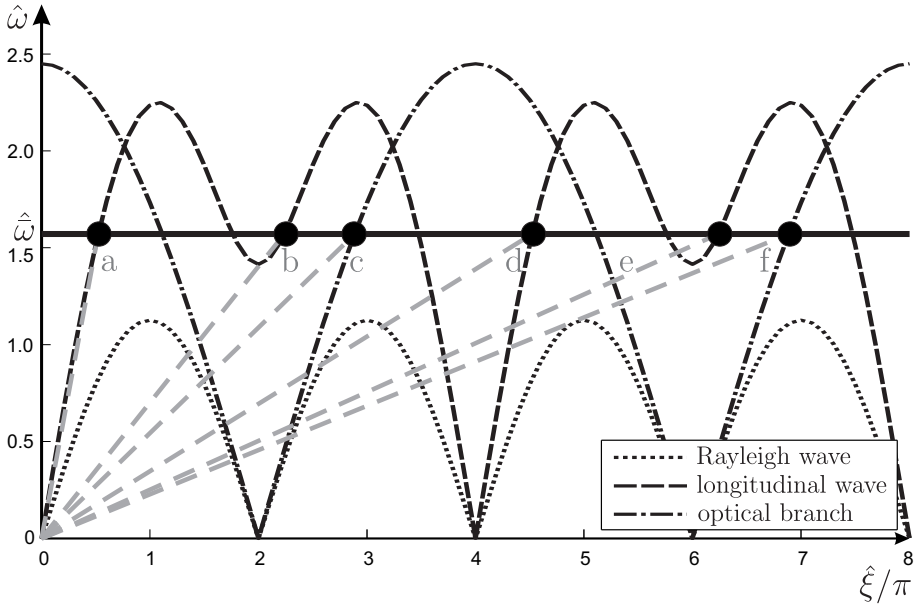

Figure 3: Dispersion curves for the infinite homogeneous triangular lattice with a semi-infinite crack, constructed according to Eqs. (12). At the fundamental radian frequency $\hat{\bar{\omega}}$ (indicated by the horizontal black line), waves can propagate with phase velocities given by the slopes of the grey rays.

The horizontal line of Fig. 3 represents the fundamental radian frequency of the applied temperature ($\hat{\bar{\omega}} = \pi/2$). It intersects the dispersion curves at a number of points, indicated by heavy dots, at which the group velocity is positive. The reason for considering only the intersections corresponding to positive group velocity comes from the fact that the energy source is located behind the crack tip. The phase velocities $\hat{v}$, identified by these intersections, are the velocities of the only waves that can travel in the lattice. They are represented by the slopes of the rays $\hat{\omega} = \hat{v}\,\hat{\xi}$, which are illustrated by dashed grey lines in Fig. 3 (these rays are infinite in number, but only the first six have been shown for clarity's sake). These phase velocities can be used to estimate the speed of crack propagation in the lattice, as discussed below.

3.3. Numerical results

The length of the crack $\hat{L}$ during time $\hat{t}$ is calculated by following the numerical procedure described in Section 2.3. In accordance with Slepyan's analytical model, the crack propagates along a straight line. The position of the crack tip, which identifies the length of the crack, is defined as the location along the $\hat{x}_1$ axis behind which all the links are broken; thus, a rupture of any link that is not adjacent to the crack tip does not alter the crack length. The results for different threshold elongations $\Delta\hat{l}_t$ are represented by solid black lines in Figs. 4a and 4b.

The velocity of each of the five crack tip trajectories illustrated in Figs. 4a and 4b is not constant, because the considered problem is nonlinear. Furthermore, the simulation of the crack propagation is performed in the transient regime, while the analytical model of Slepyan is based on the hypothesis of steady-state conditions. Similar step-like crack propagation paths have been reported in the paper by Colquitt et al. (2012) for the case of mechanical loading.

Each trajectory plotted in Figs. 4a and 4b starts with a straight line of low or null slope. This is due to the fact that the first link breaks after some time has passed, both because the elastic waves generated at the boundary need to reach the initial position of the crack tip and, above all, because energy should be accumulated in order to break the links. Note that the instant of time at which the first link breaks increases as a larger value of the threshold elongation is imposed.

It is important to observe that the links do not fail in order. It often happens that a link further from the crack tip breaks before the link that is adjacent to the crack tip. For this reason, voids appear inside the lattice. When the link closest to the crack tip attains the threshold elongation at a later time, the voids coalesce resulting in further crack growth. This phenomenon explains the jumps in the crack propagation paths. Note also that the number of jumps increases with the value of the threshold elongation. The formation and coalescence of voids have been observed in many experimental works (e.g. Broek, 1982; Benzerga and Leblond, 2010). This experimental feature is often neglected in continuum models but is a distinctive feature of the lattice model presented here.

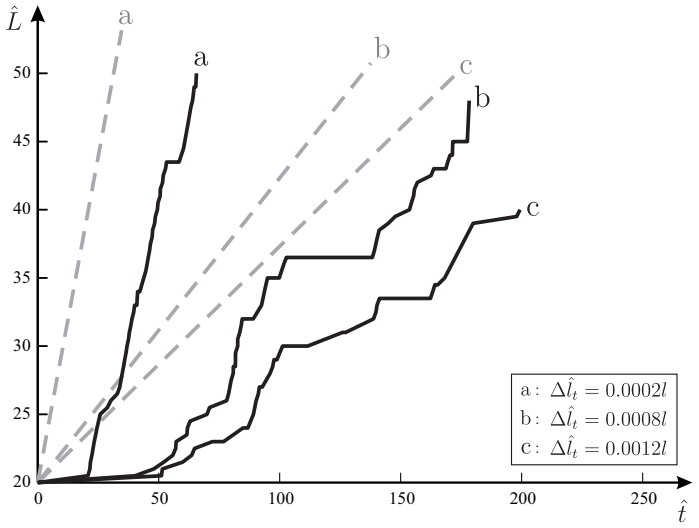

(a)

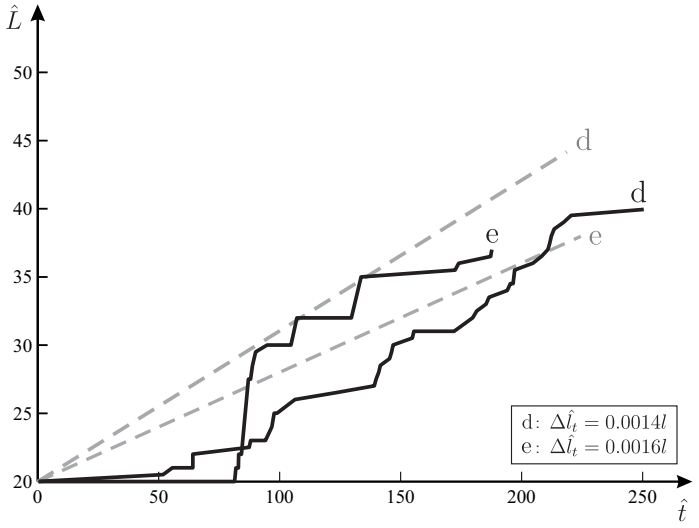

(b)

Figure 4: Crack lengths versus time for different threshold elongations $\Delta\hat{l}_t$ (solid black lines) and comparison with Slepyan's analytical model by means of the rays $\hat{L} = \hat{v}\,\hat{t} + \hat{L}_0$ (dashed grey lines), where $\hat{v}$ is the generic phase velocity determined from Fig. 3.

The crack tip trajectories shown in Figs. 4a and 4b are characterised both by jumps (due to the nucleation and successive merging of voids) and by segments between jumps, corresponding to uniform progression of the crack tip. The slopes of these segments can be approximated well by the slopes of the dashed grey rays $\hat{L} = \hat{v}\,\hat{t} + \hat{L}_0$ plotted in Figs. 4a and 4b (these are identical to those

reported in Fig. 3). This implies that the speed of uniform crack propagation can be predicted by one of the phase velocities derived from the analytical model described in Section 3.2. Moreover, excluding the initial time needed to accumulate the energy necessary to break links, the analytical phase velocities can be used to estimate the average speeds of the crack tip. In fact, from Figs. 4a and 4b it can be seen that the average speed of each path is similar to the slope of the ray labelled with the same letter.

It is apparent that the smaller the threshold elongation, the larger the average speed is, as expected. However, the highest speed in the lattice, given by the inclination angle of ray 1, cannot be exceeded. This consideration is very important, because it implies that the microstructure can be designed such that it can limit the speed of crack propagation.

4. Temperature and inertia contributions to crack propagation

In this section, the contributions of temperature and inertia to crack growth are analysed in detail. The conditions for the arrest of crack propagation are also investigated. The maximum length that may be attained by the crack will be denoted as "critical crack length".

In order to determine the temperature and inertia effects, two different problems are considered. In the first, inertia is taken into account in the equation of motion (8a) of each particle of the lattice. This case, which corresponds to the real lattice, will be referred to as the "inertial case". In the second problem, inertia is excluded from the formulation by assuming that the left-hand side term of Eq. (8a) vanishes. This case will be thus named "non-inertial case". It is worth observing that the assumption of negligible inertia can be plausibly adopted to describe many physical problems. For instance, when the temperature on the boundary varies smoothly, dynamic effects (such as the generation of elastic waves) can be ignored and, consequently, inertia can be disregarded (see, for instance, Jones (2005, 2006)).

In this section, the initial length of the crack is taken as $\hat{L}_0 = 4$, smaller than the value chosen in Section 3. This choice has been made in order to give a better description of the temperature effects on crack propagation, which are relevant near the boundary. For the same reason, an applied temperature with a lower fundamental frequency is considered. In fact, it will be shown that the size of the region where temperature effects are important increases as the fundamental frequency of the applied temperature decreases.

4.1. Temperature effects

The temperature effects are separated from the inertial effects by assuming that the mass at each node is zero (non-inertial case). Accordingly, the elongations of the links depend exclusively on the spatial temperature distribution across the lattice. This temperature distribution can be approximated by the steady-state solution of the thermal problem in the equivalent continuum, given by Eq. (A.5) in the appendix. Eq. (A.5) shows that the temperature depends

only on the coordinate x_1. The maximum and minimum values of the temperature in the steady-state regime are plotted in normalised axes in Fig. 5, where the inset figures show how the temperature changes with time at fixed values of $\hat{x}_1$.

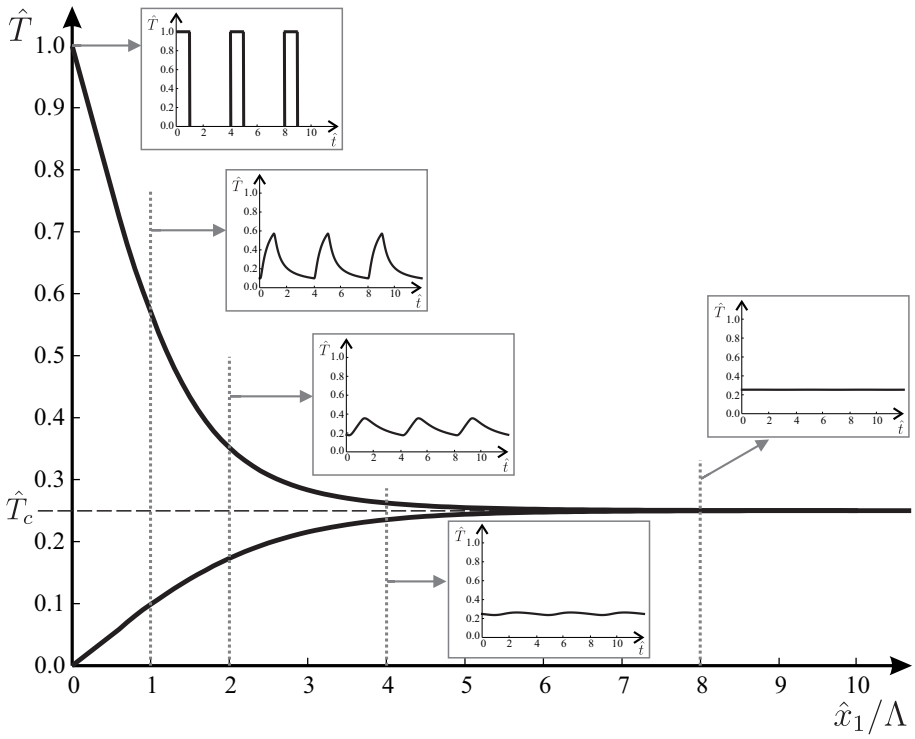

Figure 5: Normalised temperature field $\hat{T}\left(\hat{x}_1/\Lambda\right)$ in the steady-state regime, obtained through Eq. (A.5). In the insets, the time distribution of the temperature is shown at different positions $\hat{x}_1/\Lambda$.

From Fig. 5 it is apparent that there exists a region, extending from the boundary into the lattice, where temperature oscillations are significant. This region will be defined as the "region of influence". Beyond this region, the temperature is constant ($\hat{T}\left(\hat{x}_1, \hat{t}\right) = \hat{T}_c$) and equal to the average value of the boundary temperature in the period $\hat{\theta}$. It is very important to observe that the length of the region of influence increases with the thermal diffusivity of the medium and decreases with the frequency of the boundary temperature.

If the threshold elongation is attained at a temperature with an absolute value higher than the absolute value of the constant temperature $\hat{T}_c$ (consider that the boundary temperature is assumed to be negative in the numerical calculations), the crack stops propagating, reaching its critical length. The critical crack length $\hat{L}^*$ is evaluated for different values of the threshold elongation $\Delta\hat{l}_t$ and of the temperature fundamental radian frequency $\hat{\tilde{\omega}}$ using Comsol Multi-

physics ® to simulate the crack propagation process. The numerical results are shown with dots in Fig. 6. They are given for three temperature frequencies and for five threshold elongations[1]. It can be seen that, for a fixed value of the threshold elongation, the critical crack length decreases with the temperature frequency (a similar trend was observed by Jones (1999) between the maximum fluctuation of the SIF and the temperature frequency in a continuum exposed to thermal striping); on the other hand, for a given temperature frequency, the larger the threshold elongation, the smaller the critical crack length is, as expected on physical ground.

Finally, it should be pointed out that the critical crack length in the non-inertial case is independent of the initial length of the crack (provided that this is less than the critical one), since it depends only on the spatial temperature distribution across the lattice.

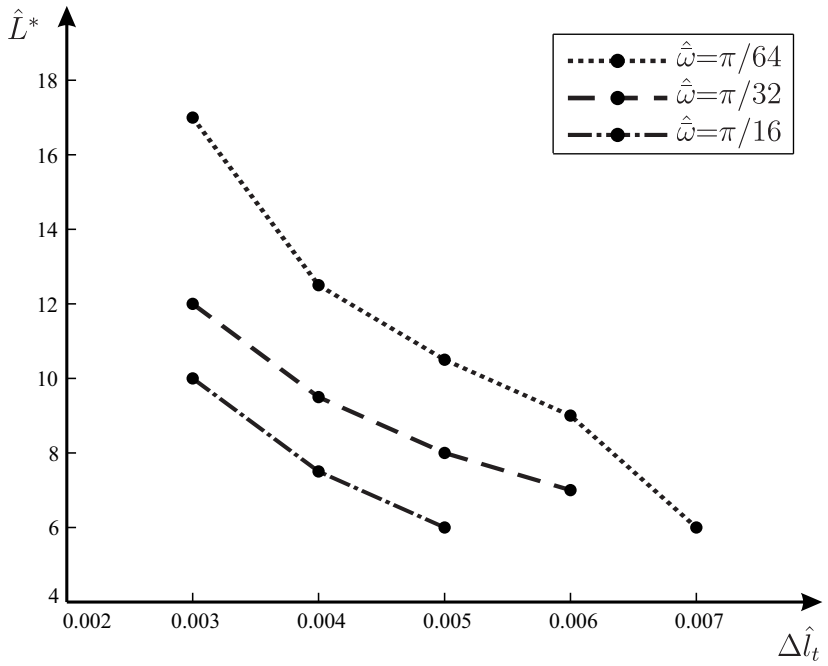

Figure 6: Dependence of the critical crack length $\hat{L}^*$ on the threshold elongation $\Delta\hat{l}_t$ of the links and on the fundamental radian frequency $\hat{\bar{\omega}}$ of the boundary temperature, in the non-inertial case.

[1]Note that the lines connecting the dots are plotted only to join the results for a given frequency. In this way, the trend of the critical crack length at a specific frequency can be seen more clearly.

4.2. Inertial effects

The effects of inertia are evaluated by comparing the time-histories of two different links in the inertial case with those obtained in the non-inertial case. This comparison is shown in Fig. 7, where the black curves are calculated without considering inertia, while the grey curves are determined by taking inertia into account. The top figures correspond to an intact lattice, while the bottom figures refer to a lattice with a non-propagating crack of length $\hat{L}_0 = 4$. The fundamental radian frequency of the applied temperature is $\hat{\bar{\omega}} = \pi/32$.

Fig. 7 shows that inertia amplifies the elongations of the links. In addition, the figure reveals that the presence of the crack amplifies the elongations of the links, especially near the crack tip (in fact, this amplification tends to disappear in the links far from the crack tip, as can be seen by comparing Fig. 7b with Fig. 7d).

From Fig. 7 it can be seen that the elongations of the links obtained in the non-inertial case decrease with the distance from the boundary. This is a consequence of the fact that the amplitude of the temperature oscillations in the region of influence decays along the $\hat{x}_1$ axis (see Fig. 5).

For the inertial case, the elastic waves generated at the boundary due to the rapid changes in temperature travel through the lattice. The frequency content of the elastic waves shown in Fig. 7 is identical to the frequency content of the temperature pulses applied on the boundary, which consists of the fundamental frequency (equal to $\hat{\bar{\omega}} = \pi/32$ in these calculations) and to its multiples. The wave components having a frequency within the pass-band (identified by the dispersion curves plotted in Fig. 3) propagate without attenuation. On the contrary, the wave components characterised by a frequency belonging to the stop-band decay exponentially. The Fast Fourier Transforms of the elastic waves represented in Figs. 7a-7d reveal that the frequencies of the harmonic components of these waves lie in the pass-band. Therefore, the wave components propagate without attenuation, but with different velocities, due to the dispersive properties of the lattice. This implies that the maximum elongation can vary in the $\hat{x}_1$ direction.

The variation of the amplitude of the elastic waves with $\hat{x}_1$, induced by the attenuation of the non-propagating waves and the dispersion of the propagating ones, is a characteristic property of the lattice, that cannot be observed in a continuum. In fact, in a continuum the elastic waves propagate with the same amplitude, because this medium is non-dispersive (see, for example, Zhelezina et al. (2006)).

Elastic waves are generated not only at the boundary, but also at points where links break. Fig. 8 shows how, in the inertial case, the elongations of two different links are increased as a consequence of the breakage of the link closest to the crack tip (here denoted as "first link"). Therefore, the elongations of the links are increased not only by the elastic waves produced by the temperature pulses at the boundary, but also by the waves created by the ruptures of the links. Actually, the waves generated by the breakages of the links do not always amplify the elongations of other links, in fact they may reduce these elongations (this depends on the position of the link and on the instant of time considered).

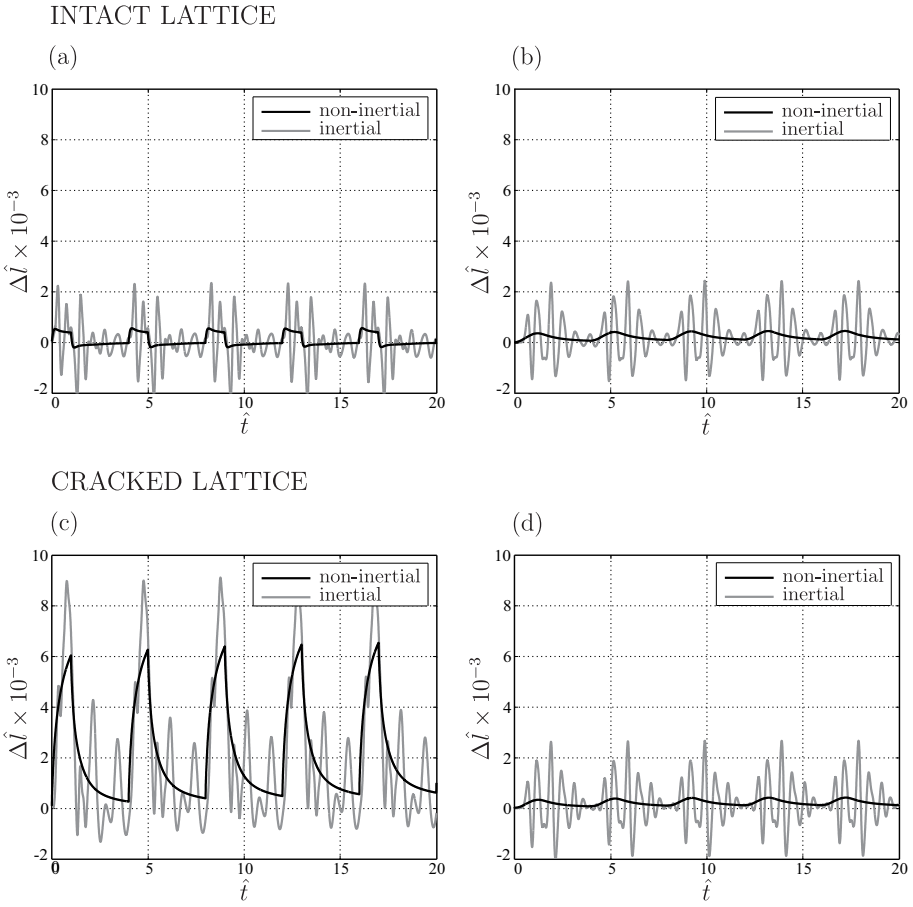

Figure 7: Time-histories of the elongations of two links in an intact lattice ((a) and (b)) and in a lattice with a non-propagating crack of length $\hat{L}_0 = 4$ ((c) and (d)). Figures (a) and (c) correspond to the inclined link located at $4 \leq \hat{x}_1 \leq 4.5$, which is adjacent to the crack tip in the cracked lattice, while figures (b) and (d) refer to a further inclined link, situated at $12 \leq \hat{x}_1 \leq 12.5$.

4.3. Critical crack length

The aim of this section is to compare the crack propagation paths determined in the inertial and non-inertial cases. This is accomplished using the numerical model of Section 2.3. For the following calculations, it is assumed that the fundamental radian frequency of the applied temperature is $\hat{\bar{\omega}} = \pi/32$ and that the threshold elongation is $\Delta\hat{l}_t = 0.005$.

The crack tip trajectories for both non-inertial and inertial cases are plotted in Fig. 9. The crosses in the two diagrams indicate the positions of the crack tip when the crack stops propagating. In both situations, the crack length tends to a finite value, which depends on the threshold elongation and on the frequency and amplitude of the temperature pulses applied on the boundary.

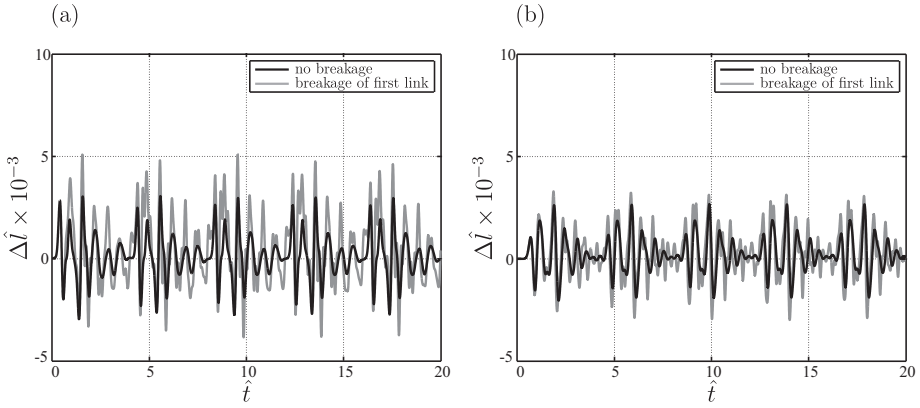

Figure 8: Time-histories of the elongations of two links, obtained in the inertial case, relative to a lattice with an initial crack of length $\hat{L}_0 = 4$, for the cases when rupture of any link is disregarded (black lines) and when the first link breaks (grey lines). Figure (a) refers to a link close to the crack tip ($6 \leq \hat{x}_1 \leq 6.5$), while figure (b) corresponds to a link further away from the crack tip ($12 \leq \hat{x}_1 \leq 12.5$).

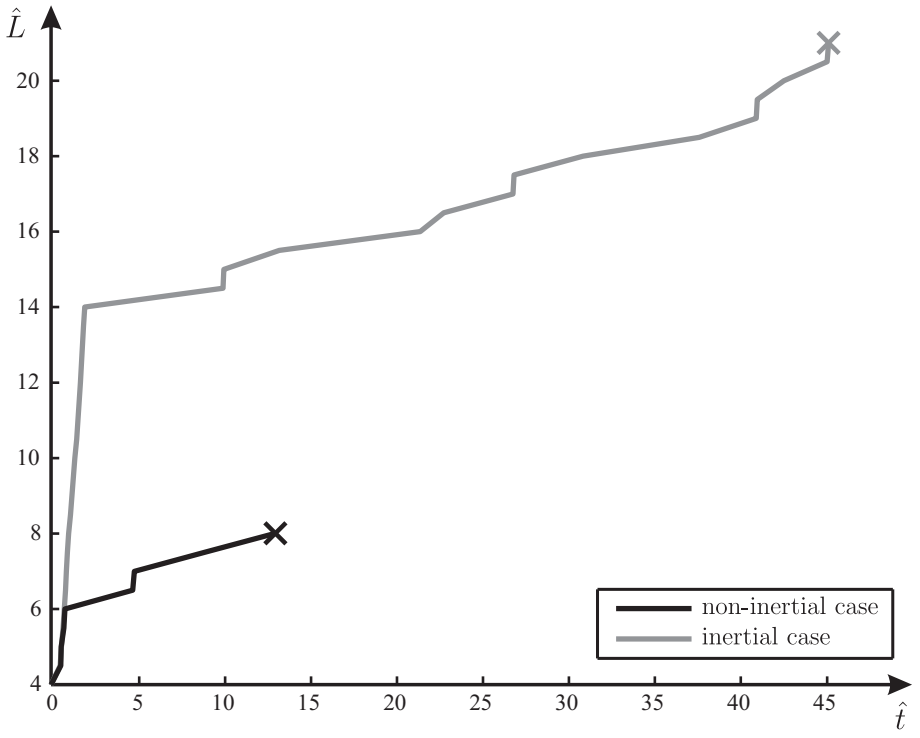

Figure 9: Crack tip trajectories in the non-inertial case (black line) and in the inertial case (grey line). For both diagrams, $\hat{\omega} = \pi/32$ and $\Delta\hat{l}_t = 0.005$.

In the non-inertial case, the crack propagation is arrested because the maximum temperature, and hence the maximum elongation induced by thermal expansion, decreases with $\hat{x}_1$ (see Fig. 5). Accordingly, crack growth stops when the maximum elongation of any link is lower than the threshold elongation, which is reached at a temperature higher than $\hat{T}_c$.

In the inertial case, the crack stops propagating because the chosen value of the threshold elongation is larger than the maximum amplitude of the elastic waves, but smaller than the value necessary to initiate crack propagation (see Fig. 7). In addition, the amplification of the elongations near the crack tip caused by the presence of the crack decreases as the crack tip advances more deeply in the lattice.

There are three main differences between the two crack tip trajectories shown in Fig. 9. First, the critical crack length for the inertial case is larger than for the non-inertial case because of the dynamic amplification of the elongations caused by inertial effects, as shown in Section 4.2. Second, it is found by detailed examination of the numerical calculations that in the inertial case the links break both in tension and in compression, while in the non-inertial case they break only in tension (this is because in compression the threshold elongation is never attained in the non-inertial case). Third, in the inertial case voids can be generated and later they can merge with the crack, while in the non-inertial case the link closest to the crack tip always breaks before the others.

In conclusion, an example has been provided, in which the crack propagation in the lattice - induced by periodic thermal excitations - is arrested.

5. Concluding remarks

Crack propagation in a homogeneous elastic triangular lattice, excited by periodic thermal shocks, has been investigated. Since the steep thermal gradients applied on the boundary of the lattice generate elastic waves, inertial effects need to be included in the formulation of the thermoelastic problem. A numerical model has been developed to analyse how an existing crack in the lattice advances.

It has been found that the crack tip does not move uniformly in the lattice. This is a consequence of the nonlinearity of the problem. However, the average speed of crack propagation can be assessed using an analytical model, which assumes that the crack propagates in a straight line with constant speed. This analytical model also provides an estimate of the maximum speed at which crack can advance through the lattice. The numerical model has also proved to be capable of predicting the formation and coalescence of voids inside the lattice.

Another interesting result is that crack propagation may be arrested, both if inertia is included or neglected. In the non-inertial case, the crack stops growing because the temperature effects are significant only in a certain region, adjacent to the boundary. In the inertial case, the crack advances further in the lattice

due to the amplification of the links' elongations caused by inertia.

Acknowledgements

G. Carta gratefully acknowledges the financial support of the Engineering and Physical Sciences Research Council (EPSRC) under the grant EP/H018239/1. M. Brun acknowledges the support of the EU FP7, grant PIEF-GA-2011-302357.

References

Benzerga, A.A., Leblond, J.-B., 2010. Ductile fracture by void growth to coalescence. Adv. Appl. Mech. 44, 169-305.

Broek, D., 1982. Elementary engineering fracture mechanics, Martinus Nijhoff Publishers, Boston.

Bueckner, H.F., 1973. Field singularities and related integral expressions in mechanics of fracture, in: Sih, G.C. (Ed.), Methods of analysis of solutions of crack problems, Vol. 1, Noordhoff International Publishing, Leyden.

Carslaw, H.S., Jaeger, J.C., 1959. Conduction of heat in solids, Oxford University Press, Oxford.

Colquitt, D.J., Nieves, M.J., Jones, I.S., Movchan, N.V., Movchan, A.B., 2012. Trapping of a crack advancing through an elastic lattice. Int. J. Eng. Sci. 61, 129-141.

Danilovskaya, V.I., 1950. Thermal stresses in an elastic half-space arising after a sudden heating of its boundary. Prikl. Mat. Mech. 14(3), 316-318.

Fineberg, J., Marder, M., 1999. Instability in dynamic fracture. Phys. Rep. 313, 1-108.

Gibiansky, E., Maz'ya, V., Movchan, A., 2005. Three-scale asymptotics for a diffusion problem coupled with the wave equation. Appl. Anal. 84(6), 585-600.

Jones, I.S., 1999. The application of a displacement controlled weight function for a single edge cracked plate to thermal fatigue damage assessment. Eng. Fract. Mech. 62, 249-266.

Jones, I.S., 2005. Impulse response model of thermal striping for hollow cylindrical geometries. Theor. Appl. Fract. Mech. 43, 77-88.

Jones, I.S., 2006. Thermal striping fatigue damage in multiple edge-cracked geometries. Fat. Fract. Eng. Mater. Struct. 29, 123-134.

Jones, I.S., Lewis, M.W.J., 1994. A frequency response method for calculating stress intensity factors due to thermal striping loads. Fat. Fract. Eng. Mater. Struct. 17(6), 709-720.

Jones, I.S., Lewis, M.W.J., 1996. An impulse response model for the prediction of thermal striping damage. Eng. Fract. Mech. 55(5), 795-812.

Marder, M., Gross, S., 1995. Origin of crack-tip instabilities. J. Mech. Phys. Solids 43(1), 1-48.

Movchan, A.B., Jones, I.S., 2006. Asymptotic and numerical study of a surface breaking crack subject to a transient thermal loading. Acta. Mech. Sin. 22, 22-27.

Nieves, M.J., Movchan, A.B., Jones, I.S., 2011. Asymptotic study of a thermoelastic problem in a semi-infinite body containing a surface-breaking crack and small perforations. Quart. J. Mech. Appl. Math. 64(3), 349-369.

Nieves, M.J., Movchan, A.B., Jones, I.S., 2012. Analytical model of thermal striping for a micro-cracked solid. Int. J. Solids Struct. 49, 1189-1194.

Nieves, M.J., Movchan, A.B., Jones, I.S., Mishuris, G.S., 2013. Propagation of Slepyan's crack in a non-uniform elastic lattice. J. Mech. Phys. Solids, DOI: 10.1016/j.jmps.2012.12.006.

Slepyan, L.I., 2001. Feeding and dissipative waves in fracture and phase transition. I. Some 1D structures and a square-cell lattice. J. Mech. Phys. Solids 49, 469-511.

Slepyan, L.I., 2001. Feeding and dissipative waves in fracture and phase transition. II. Phase-transition waves. J. Mech. Phys. Solids 49, 513-550.

Slepyan, L.I., 2001. Feeding and dissipative waves in fracture and phase transition. III. Triangular-cell lattice. J. Mech. Phys. Solids 49, 2839-2875.

Zhelezina, E., Jones, I.S., Movchan, A.B., 2006. Singular perturbation analysis of dynamic fields in a thermoelastic solid with a small surface-breaking crack. Acta. Mech. Sin. 22, 449-454.

AppendixA. Heat conduction problems in the lattice and in the equivalent continuum

In this appendix the heat conduction problems in a continuum and in a triangular lattice, both under the boundary temperature (5), are solved. Firstly, the full analytical solution (which includes both the transient and steady-state regimes) for the continuum is provided, which is then applied to the special case of steady-state conditions. Secondly, the solution in the continuum is compared with the corresponding solution in the homogenised lattice.

AppendixA.1. Solution of the heat conduction problem in the continuum

The heat conduction problem in a continuous half-space $\Omega = \{(x_1, x_2) : x_1 \geq 0\}$ of thermal diffusivity κ^* can be stated as follows:

$$\kappa^* \frac{\partial^2 T(x_1,t)}{\partial x_1^2} = \frac{\partial T(x_1,t)}{\partial t} \qquad \text{for } x_1 > 0, t > 0; \tag{A.1a}$$

$$T(x_1,t) = T_{ext}(t) + T_{ref} \qquad \text{for } x_1 = 0, t > 0; \tag{A.1b}$$

$$T(x_1,t) \to T_{ref} \qquad \text{for } x_1 \to \infty, t > 0; \tag{A.1c}$$

$$T(x_1,t) = T_{ref} \qquad \text{for } x_1 \geq 0, t = 0. \tag{A.1d}$$

In the formulae above, T_{ext} represents the variation of temperature, applied on the boundary, with respect to the ambient temperature T_{ref}. In this paper, it is assumed for simplicity that $T_{ref} = 0$. Moreover, with respect to the elastic problem in the lattice described in Section 2.1, it is assumed that T_{ref} is equal to the stress-free temperature of the body.

The initial boundary value problem defined by Eqs. (A.1) remains valid also for a continuum with a crack, if the crack is assumed to be perfectly thermally-conducting. It is worth noticing that the temperature T is independent of the coordinate x_2, as the external temperature T_{ext} is assumed to be uniform along the x_2 axis.

For the particular boundary temperature specified by Eq. (5), the temperature field $T(x_1, t)$ in the continuum is given by Eq. (6). The normalised temperature field $T(x_1/\sqrt{\kappa^*\tau}, t/\tau)/T_0$ is plotted in Fig. A.1. Fig. A.1 shows that the temperature decays fast in space and, in addition, that the steady-state regime is reached after few cycles.

AppendixA.2. Steady-state solution of the heat conduction problem in the continuum

For a time-harmonic temperature of radian frequency $\tilde{\omega}$ and amplitude $\tilde{T}_0$ applied on the boundary of a semi-infinite continuum $\Omega = \{(x_1, x_2) : x_1 \geq 0\}$ of thermal diffusivity κ^*, the heat conduction problem is:

$$\kappa^* \frac{\mathrm{d}^2 \tilde{T}(x_1)}{\mathrm{d}x_1^2} = \mathrm{i}\,\tilde{\omega}\,\tilde{T}(x_1) \qquad \text{for } x_1 > 0; \tag{A.2a}$$

$$\tilde{T}(x_1) = \tilde{T}_0 \qquad \text{for } x_1 = 0; \tag{A.2b}$$

$$\tilde{T}(x_1) \to 0 \qquad \text{for } x_1 \to \infty. \tag{A.2c}$$

The solution of this problem is given by (see, for example, Carslaw and Jaegar (1959))

$$\tilde{T}(x_1) = \tilde{T}_0\, \mathrm{e}^{-\sqrt{\tilde{\omega}/2\kappa^*}(1+\mathrm{i})x_1}. \tag{A.3}$$

The steady-state solution of the thermal problem (A.1) can be obtained by decomposing the boundary temperature in Fourier series and by applying

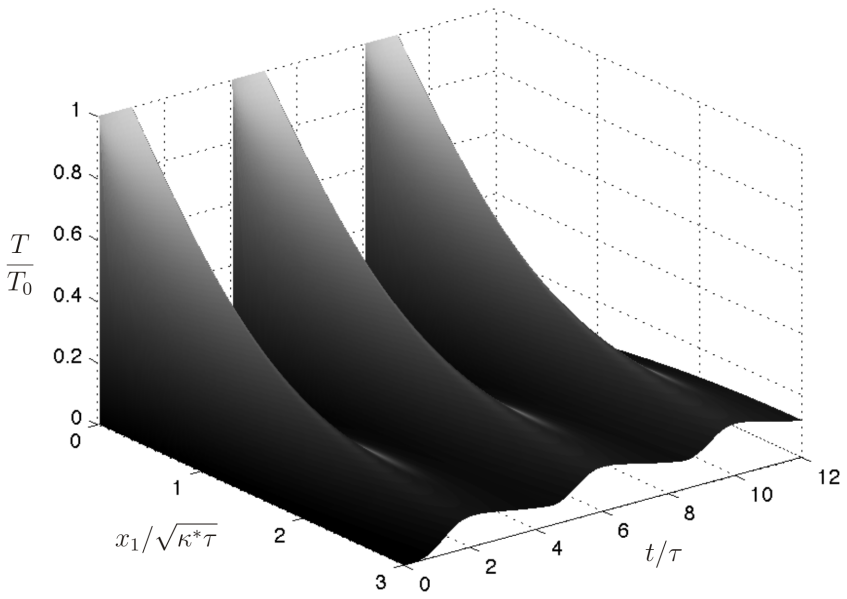

Figure A.1: Normalised temperature distribution in a semi-infinite continuum under the boundary temperature (5) (with $\theta = 4\,\tau$).

Fourier analysis with the help of Eqs. (A.2) and (A.3). The Fourier series of the boundary temperature (5) is given by

$$T_{ext}(t) = \sum_{n=-\infty}^{\infty} \frac{\mathrm{i}T_0}{2n\pi} \left(\mathrm{e}^{-\mathrm{i}n\omega\tau} - 1\right) \mathrm{e}^{\mathrm{i}n\omega t}, \tag{A.4}$$

where $\omega = 2\pi/\theta$ is the fundamental radian frequency of the boundary temperature. The solution in the steady-state regime is thus found by linear superposition:

$$\begin{aligned} T(x_1,t) = &\sum_{n=-\infty}^{\infty} \frac{\mathrm{i}T_0}{2n\pi} \left(\mathrm{e}^{-\mathrm{i}n\omega\tau} - 1\right) \mathrm{e}^{-\sqrt{\frac{|n\omega|}{2\kappa^*}}[1+\mathrm{sgn}(n)\mathrm{i}]x_1} \mathrm{e}^{\mathrm{i}n\omega t} \\ =&\frac{T_0\tau}{\theta} + \frac{T_0}{\pi} \sum_{n=1}^{\infty} \frac{\mathrm{e}^{-\sqrt{\frac{n\omega}{2\kappa^*}}x_1}}{n} \\ &\times \left\{ \sin\left[n\omega(t-\tau) + \sqrt{\frac{n\omega}{2\kappa^*}}x_1\right] + \sin\left[n\omega t - \sqrt{\frac{n\omega}{2\kappa^*}}x_1\right] \right\}, \end{aligned} \tag{A.5}$$

where $\mathrm{sgn}(\cdot)$ is the sign function.

AppendixA.3. Solution of the heat conduction problem in the lattice

The heat conduction problem in the semi-infinite lattice depicted in Fig. 1a is solved numerically. To this aim, the semi-infinite lattice is approximated by a finite lattice of width B and height H, the horizontal and the right boundaries of which are assumed to be adiabatic (see Fig. 1b).

For convenience, the nodes of the lattice are grouped into the following sets:

$$\bullet \text{ interior domain}: \quad \Gamma = \left\{ \mathbf{p} : x_1(\mathbf{p}) > 0, -(n_2+1)\frac{\sqrt{3}}{2}l < x_2(\mathbf{p}) < n_2\frac{\sqrt{3}}{2}l \right\}; \tag{A.6a}$$

$$\bullet \text{ left boundary}: \quad \gamma_l = \left\{ \mathbf{p} : x_1(\mathbf{p}) = 0, -(n_2+1)\frac{\sqrt{3}}{2}l \le x_2(\mathbf{p}) \le n_2\frac{\sqrt{3}}{2}l \right\}; \tag{A.6b}$$

$$\bullet \text{ right boundary}: \quad \gamma_r = \left\{ \mathbf{p} : x_1(\mathbf{p}) = B, -(n_2+1)\frac{\sqrt{3}}{2}l \le x_2(\mathbf{p}) \le n_2\frac{\sqrt{3}}{2}l \right\}; \tag{A.6c}$$

$$\bullet \text{ top boundary}: \quad \gamma_t = \left\{ \mathbf{p} : 0 < x_1(\mathbf{p}) < B, x_2(\mathbf{p}) = n_2\frac{\sqrt{3}}{2}l \right\}; \tag{A.6d}$$

$$\bullet \text{ bottom boundary}: \quad \gamma_b = \left\{ \mathbf{p} : 0 < x_1(\mathbf{p}) < B, x_2(\mathbf{p}) = -(n_2+1)\frac{\sqrt{3}}{2}l \right\}; \tag{A.6e}$$

$$\bullet \text{ near the crack}: \quad \gamma_c = \left\{ \mathbf{p} : 0 \le x_1(\mathbf{p}) \le L_0, x_2(\mathbf{p}) = 0, -\frac{\sqrt{3}}{2}l \right\}. \tag{A.6f}$$

In the equations above, n_2 represents the number of rows above and below the crack.

The thermal problem in the lattice (in which the top, bottom and right boundaries are considered to be adiabatic, the temperature (5) is applied on the left boundary and the crack is assumed to be perfectly thermally-conducting) can be stated as follows:

$$\frac{\partial T(\mathbf{p},t)}{\partial t} = \frac{\kappa}{l^2}\left[\sum_{n=1}^{N(\mathbf{p})} T(\mathbf{q}_n,t) - N(\mathbf{p})T(\mathbf{p},t)\right] \quad \text{for } \mathbf{p}\in\Gamma, t>0; \tag{A.7a}$$

$$T(\mathbf{p},t) = T_{ext}(t) + T_{ref} \quad \text{for } \mathbf{p}\in\gamma_l, t>0; \tag{A.7b}$$

$$T(\mathbf{p},t) = \frac{1}{N(\mathbf{p})}\sum_{n=1}^{N(\mathbf{p})} T(\mathbf{q}_n,t) \quad \text{for } \mathbf{p}\in\gamma_r\cup\gamma_t\cup\gamma_b, t>0; \tag{A.7c}$$

$$T(\mathbf{p},t) = T_{ref} \quad \text{for } \forall\mathbf{p}, t=0. \tag{A.7d}$$

Also for the lattice, it is assumed that $T_{ref}=0$.

The thermal problem defined by Eqs. (A.7) is solved by making use of the Finite Difference Method. Convergence studies indicate that a suitable time step is 0.02τ. It is found that the temperature distribution does not vary significantly in the x_2 direction (more precisely, the maximum difference between the values of temperature at any two points with the same x_1 and different x_2 values is less than 1% of T_0). Consequently, this problem can be considered as one-dimensional, as in Eqs. (A.1).

The spatial profiles of the temperature in the lattice at two different times are shown with dots in Fig. A.2. The dots represent the values obtained at the

nodal points of the lattice. The solid grey lines plotted in the same figure indicate instead the temperature profiles of the equivalent continuum, obtained from Eq. (6). In order to compare the solutions relative to the lattice and the continuum, the properties of the continuum should correspond to the homogenised properties of the lattice. For this reason, the thermal diffusivity κ of the lattice links has been taken as $\kappa = \kappa^*/\sqrt{3}$, where κ^* is the thermal diffusivity of the continuum.

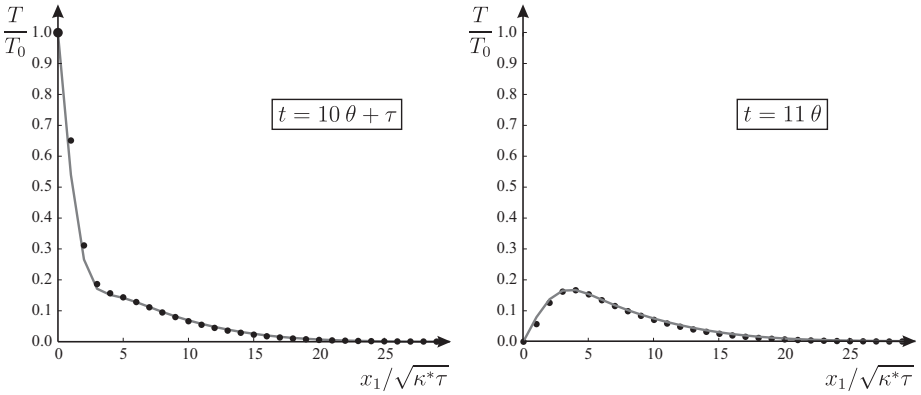

Figure A.2: Spatial temperature profiles of the lattice (dots) and of the equivalent continuum (solid grey lines) at two different times (with $l/\sqrt{\kappa^*\tau} = 1$, $B = 80\,l$, $n_2 = 10$, $\theta = 4\,\tau$).

From Fig. A.2 it is apparent that there is a very good correspondence between the solutions of the heat conduction problems in the lattice and in the equivalent continuum. This observation justifies the use of Eq. (6) in the numerical simulation of the thermoelastic problem for the lattice (see Section 2.3).

List of figures captions

Figure 1: (a) Semi-infinite triangular lattice with a finite edge crack of length L_0. (b) Schematic drawing of the finite lattice modelled in the numerical simulations, which approximates the semi-infinite lattice in (a). Adiabatic boundary conditions and Perfectly Matched Layers (PMLs) are introduced in the model. Γ is the domain of width B and height H, while γ_l, γ_r, γ_t, γ_b and γ_c are the left, right, top, bottom and crack boundaries, respectively.

Figure 2: Time variation of the temperature imposed on the boundary $x_1 = 0$ of the lattice (with $\theta = 4\,\tau$).

Figure 3: Dispersion curves for the infinite homogeneous triangular lattice with a semi-infinite crack, constructed according to Eqs. (12). At the fundamental radian frequency $\hat{\bar{\omega}}$ (indicated by the horizontal black line), waves can propagate with phase velocities given by the slopes of the grey rays.

Figure 4: Crack lengths versus time for different threshold elongations $\Delta\hat{l}_t$ (solid black curves) and comparison with Slepyan's analytical model by means of the rays $\hat{L} = \hat{v}\,\hat{t} + \hat{L}_0$ (dashed grey curves), where $\hat{v}$ is the generic phase velocity determined from Fig. 3.

Figure 5: Normalised temperature field $\hat{T}\,(\hat{x}_1/\Lambda)$ in the steady-state regime, obtained through Eq. (A.5). In the insets, the time distribution of the temperature is shown at different positions $\hat{x}_1/\Lambda$.

Figure 6: Dependence of the critical crack length $\hat{L}^*$ on the threshold elongation $\Delta\hat{l}_t$ of the links and on the fundamental radian frequency $\hat{\bar{\omega}}$ of the boundary temperature, in the non-inertial case.

Figure 7: Time-histories of the elongations of two links in an intact lattice ((a) and (b)) and in a lattice with a non-propagating crack of length $\hat{L}_0 = 4$ ((c) and (d)). Figures (a) and (c) correspond to the inclined link located at $4 \leq \hat{x}_1 \leq 4.5$, which is adjacent to the crack tip in the cracked lattice, while figures (b) and (d) refer to a further inclined link, situated at $12 \leq \hat{x}_1 \leq 12.5$.

Figure 8: Time-histories of the elongations of two links, obtained in the inertial case, relative to a lattice with an initial crack of length $\hat{L}_0 = 4$, for the cases when rupture of any link is disregarded (black lines) and when the first link breaks (grey lines). Figure (a) refers to a link close to the crack tip ($6 \leq \hat{x}_1 \leq 6.5$), while figure (b) corresponds to a link further away from the crack tip ($12 \leq \hat{x}_1 \leq 12.5$).

Figure 9: Crack tip trajectories in the non-inertial case (black line) and in the inertial case (grey line). For both diagrams, $\hat{\bar{\omega}} = \pi/32$ and $\Delta\hat{l}_t = 0.005$.

Figure A.1: Normalised temperature distribution in a semi-infinite continuum under the boundary temperature (5) (with $\theta = 4\,\tau$).

Figure A.2: Spatial temperature profiles of the lattice (dots) and of the equiv-

alent continuum (solid grey lines) at two different times (with $l/\sqrt{\kappa^* \tau} = 1$, $B = 80\, l$, $n_2 = 10$, $\theta = 4\, \tau$).